

PAPER

Active near-field plasmonic switches based on Sierpiński-fractal nanoantennas on VO₂ films


To cite this article: Yashna Sharma and Anuj Dhawan 2022 *J. Opt.* **24** 065001

View the [article online](#) for updates and enhancements.

You may also like

- [Dielectric optical nanoantennas](#)
Md Rabiul Hasan and Olav Gaute Hjeltnes
- [Numerical investigation of plasmonic bowtie nanorings with embedded nanoantennas for achieving high SEIRA enhancement factors](#)
Aakansha Suchitta and Anuj Dhawan
- [Exploiting metamaterials, plasmonics and nanoantennas concepts in silicon photonics](#)
Francisco J Rodríguez-Fortuño, Alba Espinosa-Soria and Alejandro Martínez

Active near-field plasmonic switches based on Sierpiński-fractal nanoantennas on VO₂ films

Yashna Sharma¹  and Anuj Dhawan^{2,*} 

¹ Department of Electronics and Communication Engineering, Delhi Technological University, Delhi, India

² Department of Electrical Engineering, Indian Institute of Technology Delhi, New Delhi, India

E-mail: adhawan@ee.iitd.ac.in

Received 15 January 2022, revised 15 March 2022

Accepted for publication 29 March 2022

Published 28 April 2022



Abstract

We propose active near-field plasmonic switches based on a Sierpiński-fractal contour-bowtie plasmonic nanoantenna on top of a VO₂ (vanadium-dioxide) thin film. The near-field intensity of the proposed fractal plasmonic nanoantenna can be switched by the application of heat, voltage, or optical energy to the underlying VO₂ layer, which leads to a phase change of VO₂ from the semiconductor state to the metallic state. This phase transition of the underlying VO₂ film leads to an overall change in the optical properties of the nanoantenna system, hence driving the switch from an OFF state (with low near-field intensity) to an ON state (with high near-field intensity). The near-field switching ability of the proposed switch is quantified by the intensity switching ratio (ISR), i.e. the ratio of the intensity between the two arms of plasmonic nanoantenna in its ON state to its OFF state ($I_{\text{ON}}/I_{\text{OFF}}$). Finite difference time domain simulations were employed to calculate the ISR of the proposed near-field plasmonic switches. As the fractal order of the Sierpiński-fractal contour-bowtie nanoantenna is increased, the intensity in the 'ON' state of the switch is enhanced along with a reduction of intensity in the 'OFF' state of the switch. Thus, higher fractal orders of the Sierpiński-fractal contour-bowtie plasmonic nanoantenna lead to very high values of the ISR for the proposed near-field switch. We demonstrate an ISR of ~ 900 with a fractal order of 2 for the proposed switch which is the highest value of near-field ISR reported thus far for a near-field plasmonic switch. Further, we also demonstrate that the ISR and the spectral response of the proposed near-field switch can be controlled by changing its structural parameters such as the length of the nanoantenna arm, the contour thickness, and the thickness of VO₂ layer.

Supplementary material for this article is available [online](#)

Keywords: active switching, near-field switching, plasmonics, Sierpiński fractal, nanoantennas, vanadium dioxide

(Some figures may appear in color only in the online journal)

* Author to whom any correspondence should be addressed.

1. Introduction

The coupling of incident light to the collective oscillations of electrons at the interface of a metal and a dielectric leads to the generation of propagating surface waves called surface plasmon polaritons [1, 2]. In addition, when light interacts with a metallic nanostructure such as a nanoparticle, the conduction electrons of the nanoparticle exhibit non-propagating collective oscillations known as the **localized surface plasmons (LSPs)** [1, 2]. The proper engineering of these metallic nanostructures can lead to the formation of intense electromagnetic hotspots with sub-wavelength confinement. In the recent years, these metallic nanostructures have been employed extensively in the fields of nanoplasmonics [3] and plasmonic metamaterials [4–6]. Further, the discovery and development of new material platforms such as **tunable materials** [7, 8] and **near-zero index materials** [9] have significantly advanced the research in these areas. **One of the primary applications of nanoplasmonics is plasmonic nanoantennas which are capable of transferring the electromagnetic energy from the near-field to the far-field in the transmitting mode, and vice versa in the receiving mode** [10–12]. Plasmonic nanoantennas have been employed for various applications in the past such as surface enhanced Raman spectroscopy [13], fluorescence enhancement [14], and others [15, 16].

In recent years, several plasmonic nanoantennas based on fractal structures—such as the Sierpiński carpet, Sierpiński triangles, Cayley tree, ternary tree, Koch fractal and others [17–23]—have been proposed. It has been demonstrated that the fractal versions of the plasmonic nanoantennas exhibit multiple advantages such as a higher electromagnetic enhancement [19], a broadband spectral response [22], miniaturization of the antenna size [24] and tunability of the plasmon resonance wavelength [21]. Due to these advantages, the plasmonic fractal nanoantennas have been employed for various applications [25–28]. However, the use of these plasmonic fractal nanoantennas for active plasmonic switching has not been explored so far.

The design of all-optical plasmonic switches is critical for the implementation of photonic integrated circuits [29, 30] as they offer the possibility of controlling and manipulating light at the nanoscale through another optical signal. Numerous plasmonic switches based on far-field switching of transmission, reflection, or extinction spectra of plasmonic nanoantennas have been proposed in the past [31, 32]. However, there have been limited reports where the near-field intensity of a plasmonic nanoantenna has been actively switched [33, 34]. The control and switching of the near-field intensity of a plasmonic nanoantenna is particularly important for applications such as particle trapping and tweezing [35], design of vortex beams [36], non-linear optics [37], switchable lasing [38] and others. These plasmonic switches can be integrated into photonic integrated chips to be employed for telecommunication applications [39, 40]. Further, these switches can also be integrated into plasmonic integrated circuits [30] and plasmonic logic circuits [41] which can be employed for optical computation and optical data storage [42].

In this paper, we demonstrate active near-field plasmonic switches based on a Sierpiński-fractal contour-bowtie plasmonic nanoantenna on top of a VO₂ (vanadium-dioxide) coated SiO₂ substrate (figure 1). This paper demonstrates, for the first time, the use of a plasmonic fractal nanoantenna for active switching of the near-field intensity. The proposed switch does not require shaping [43, 44] or complex manipulation of the incident laser beam to achieve near-field switching. The active near-field intensity switching is achieved by the placing the nanoantenna on a thin layer of vanadium dioxide (VO₂)—a phase change material.

VO₂ is a phase change material that exhibits an ultrafast reversible phase transition from being a transparent semiconductor at room temperature to a highly reflective metal on exposure to heat, voltage, or optical energy [45–53]. When undoped VO₂ is heated above its semiconductor to metal transition temperature of 68 °C, it transforms from a meta-stable monoclinic phase to a stable tetragonal phase [47]. When VO₂ undergoes a transformation from its monoclinic to its tetragonal structure, it leads to a change in the real (n) and imaginary part (k) of its refractive index. This change in the refractive index is manifested as a change in the optical properties of VO₂ as it undergoes a phase transition.

In recent years, there have been a few reports of near-field switches that employ either nanoantennas made from only VO₂ [54], plasmonic nanoantennas based on photoconductive materials [55], or a combination of plasmonic nanoantennas and VO₂ layers [33, 56]. Although near-field switching by employing a combination of plasmonic nanoantennas and VO₂ films has been reported by a few researchers, those switches were based on non-fractal designs of the plasmonic nanoantennas. In this paper, we demonstrate near-field intensity switching by employing a Sierpiński-fractal contour-bowtie plasmonic nanoantenna on top of a VO₂ thin film. Bowtie-based plasmonic nanoantennas were chosen as bowtie nanoantennas are compatible with the Sierpiński-triangle fractal geometry [17, 18, 20], and fabrication processes are available for fabricating such Sierpiński fractal nanostructures [17]. To exploit the advantage of high EM enhancement which can be achieved using bowtie nanoantennas [57] and to simultaneously provide an increased area for interaction with the underlying VO₂ layer, we employed a variation of the standard bowtie nanoantenna—a contour-bowtie plasmonic nanoantenna, i.e. a bowtie nanoantenna with a central hollow cavity—as the basis shape for designing this fractal nanoantenna based near-field switch.

The schematic of the plasmonic fractal nanoantenna based near-field switch is shown in figure 1. **It is well known that a fractal is a shape which is self similar, and can be represented by a basis shape along with a transformation rule that can be applied iteratively on the basis shape to obtain higher fractal orders.** A well known fractal design is based on the Sierpiński triangle whose basis shape is a triangle. In this work, we propose a variation of the Sierpiński triangle where a triangle with a hollow cavity, i.e. a contour-triangle is taken as the basis shape. The thickness of the gold contour is taken as ‘ c ’ nm (figure 1). In the first iteration, the original contour-triangle

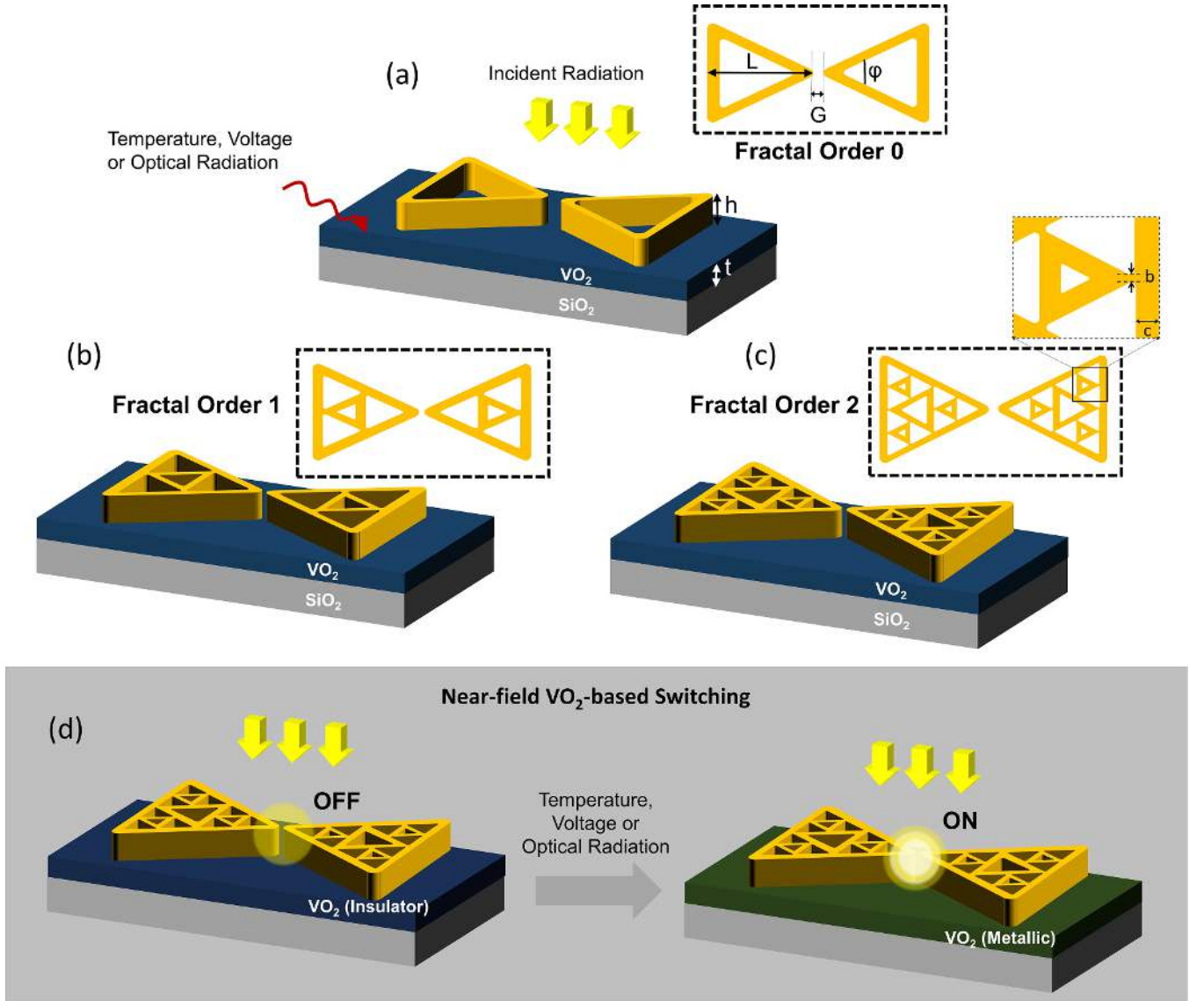


Figure 1. Schematic of the proposed Sierpiński-fractal contour-bowtie plasmonic nanoantenna on VO_2 for active near-field switching. (a) Fractal order 0, i.e. non-fractal structure showing the contour-bowtie as the basis shape, (b) fractal order 1 and (c) fractal order 2 of the proposed Sierpiński-fractal contour-bowtie plasmonic nanoantenna. The hollow triangular pillars have a length ' L ' and height ' h ', and are separated from each other by a gap ' G '. The flare angle ' φ ' of the nanoantenna is fixed at 60° for all the simulations. The thickness of the contour is ' c ' and the bridge width is ' b '. (d) Mechanism of near-field VO_2 based switching showing the transition of the Sierpiński-fractal contour-bowtie plasmonic nanoantenna from the 'OFF' state with VO_2 (S) to 'ON' state with VO_2 (M) on exposure to temperature, voltage or optical radiation.

(fractal order 0) is replaced with three contour-triangles, such that each of the smaller triangles has a side length which is half of the side length of the original triangle, and these are arranged along the outline of the original triangle. In the second iteration, the same transformation rule is applied to each of the smaller hollow triangles. The flare angle of the nanoantenna (φ) is kept constant at 60° for all the iterations. Two fractal triangular gold pillars, each with a length ' L ' and height, ' h ', are placed face to face with a gap ' G ' between them in order to form a Sierpiński-fractal contour-bowtie nanoantenna. This fractal nanoantenna is placed on top of a VO_2 layer of thickness ' t ' as shown in figure 1(a). It must be noted that in an ideal Sierpiński-type fractal design, the corners of

the inner triangular components touch the outer triangle at a single point, creating a geometric singularity. However, the fabrication of such fractal features with singularities cannot be achieved with state-of-the-art nanolithography techniques. Therefore, to avoid the singularity issues and allow conductive coupling in the antenna components [24, 58], we have considered a structure where all the corners are sufficiently rounded as shown in figure 1(c). It must be noted that theoretically, the fractal design of such a structure can be iterated infinitely, however, it is limited by the minimum feature size achievable with the state-of-the-art fabrication techniques. Therefore, we analyze the active near-field switching properties of the proposed switch up to the second fractal order only.

The switching is achieved in this plasmonic fractal nanoantenna based near-field switch by applying heat, voltage, or optical energy to the underlying VO₂ layer, which leads to a phase change of VO₂ from the semiconductor state to the metallic state, leading to an overall change in the optical properties of the nanoantenna system (see figure 1(d)). At the visible and the near infra-red wavelengths, the near-field intensity between the two arms of the contour-bowtie nanoantenna is very low for the case when VO₂ is in its semiconductor state. This is equivalent to the OFF state of the switch. However, as VO₂ transforms from its semiconductor phase to its metallic phase, an intense electromagnetic hotspot is created at the center of the plasmonic nanoantenna, thus, driving the switch into its ON state. The near-field switching ability of the proposed switch is measured by the intensity switching ratio (ISR), i.e. the ratio of the intensity at the center of the plasmonic nanoantenna in its ON state to that in its OFF state ($I_{\text{ON}}/I_{\text{OFF}}$). As the fractal order of the contour-bowtie nanoantenna is increased, the intensity in the 'ON' state of the switch is enhanced. Moreover, the intensity in the 'OFF' state of the switch is decreased as the fractal order increases. This simultaneous enhancement of intensity in the 'ON' state and reduction of intensity in the 'OFF' state with an increase in the fractal order leads to very high values of the ISRs for higher fractal orders, thereby making these Sierpiński-fractal contour-bowtie plasmonic nanoantennas suitable for efficient near-field optical switching. Moreover, as the underlying VO₂ layer is capable of being switched at femtosecond time scales [52, 53], these switches can potentially be employed for ultra-fast active near-field switching.

A comparison with the previously reported values of the near-field ISR reveals that the proposed switch has a significantly better performance than the previously reported near-field plasmonic switches. Previously, an ISR of 5.6 has been reported by employing VO₂ dipole nanostructures on Au substrates [54], an ISR of 7 has been reported by employing Au dipole nanoantennas with a VO₂-filled cavity [56], an ISR of 12 has been achieved using dipole nanoantenna with a photoconductive gap [55], and an ISR of ~80 has been demonstrated by employing ring-rhombus nanoantenna [33]. In this paper, we report that a ISR as high as ~900 can be achieved by increasing the fractal order of the proposed switch to 2. The ISR reported in this paper (~900) is the highest value of ISR reported thus far for a near-field plasmonic switch.

In this paper, finite difference time domain (FDTD) method was used to exhaustively analyze the performance of the proposed plasmonic fractal nanoantenna-based near-field switches. The effect of the structural parameters—such as the fractal order, the length of the nanoantenna arm, the thickness of the contour, and the thickness of VO₂ layer—on the ISR and the wavelength of maximum switching (i.e. the wavelength at which maximum ISR is achieved) is numerically analyzed.

2. Methods

Numerical modeling based on the FDTD method was employed for the calculation of electromagnetic fields in the

proposed switch. FDTD converts the continuous time Maxwell's equations to difference equations, and employs the Yee's algorithm to solve them for both electric and magnetic fields simultaneously by discretization of space and time into grids [59]. A 3D electromagnetic solver (Lumerical FDTD Solutions) by Lumerical Solutions Inc. was employed for this work. A uniform grid size of 1 nm in the x -, y - and z -directions was used over the entire simulation area. It must be noted that the value of grid size was chosen after carrying out exhaustive convergence testing. Perfectly matched layer boundaries were used in the x -, y -, and z -directions. A broadband plane wave source was incident on the structure from the top (figure 1) with a wavelength range from 600 to 2000 nm. The incident light was taken to be linearly polarized along the antenna axis. The optical constants of gold and vanadium dioxide (VO₂) employed for this work are given in the supplementary information (supplementary information, note 1 available online at stacks.iop.org/JOpt/24/065001/mmedia). These material constants were used after carrying out appropriate fitting in the desired wavelength range.

These near-field switches based on the Sierpiński-fractal contour-bowtie plasmonic nanoantenna can be fabricated by growing a thin layer of VO₂ on a SiO₂ substrate by employing thin film deposition processes such as pulsed laser deposition [60] or sputter deposition [61] (see figure S2, supplementary information, note 2). Subsequently, a thin layer of gold can be deposited on top of the VO₂ thin film using either sputter deposition or electron beam evaporation. The Sierpiński-fractal contour-bowtie plasmonic nanoantennas can be fabricated by milling hollow cavities—employing helium ion milling [62] or transmission electron beam ablation lithography (TEBAL) [63]—to create a contour-bowtie design with the required triangular fractal features. However, the fabrication of fractal features with sharp corners or singularities is not feasible using these processes. Thus, the etched triangular features are expected to have rounded corners. This leads to a Sierpiński contour-bowtie fractal where the inner gold contour triangles merge into the outer contour triangles with a bridge width ' b ' dependent on the rounding radius of the etched triangles (see figure 1(c)). It is imperative to have a non-zero bridge width to avoid the singularity issues and also to allow conductive coupling in the antenna components. Therefore, we have accounted for the rounding radius of the etched triangles as well as the bridge width ' b ' in our FDTD simulations. The rounding radius has been taken as 3 nm in all the simulations carried out in this paper, which leads to a bridge width of ~5 nm. The primary limitation of the Sierpiński-fractal contour-bowtie nanoantennas proposed in this paper is the requirement of sophisticated fabrication processes for fabricating plasmonic nanoantennas having higher fractal orders. Most of these processes such as helium ion milling [51] or TEBAL [63] have low fabrication rates. In order to overcome these limitations, fabrication processes such as bio-fabrication using deoxyribonucleic acid (DNA) origami [64] and extreme ultraviolet (UV) lithography [65] could be potentially employed to fabricate the fractal nanoantennas with sub 20 nm features.

In this paper, we have carried out the FDTD simulations to analyze the performance of the proposed nanoantennas. The effect of the different structural parameters on the ISR and the wavelength of maximum ISR is numerically analyzed. Figure 1(a) shows two fractal-triangular gold nanopillars, each with an arm length ' L ' that are placed face to face with a gap ' G ' between them in order to form a Sierpiński-fractal contour-bowtie nanoantenna. The thickness of the gold contour of the nanoantenna is taken as ' c ' nm. This fractal nanoantenna is placed on top of a VO₂ layer of thickness ' t ' as shown in figure 1(a). The effect of the varying these structural parameters on the ISR and the wavelength of maximum ISR is numerically analyzed in this paper. For this analysis, the length of the nanoantenna arm is varied from 250 to 375 nm, the thickness of the VO₂ layer is varied from 10 to 100 nm, and the contour thickness of the nanoantenna arms is varied from 10 to 30 nm.

3. Results and discussion

FDTD simulations were carried out to numerically obtain the near-field E -field enhancement ($|\mathbf{E}|/|\mathbf{E}_0|$) and the near-field intensity enhancement ($|\mathbf{E}|^2/|\mathbf{E}_0|^2$) where \mathbf{E} is the E -field at the center of the nanoantenna and \mathbf{E}_0 is the incident E -field. These numerical simulations were carried out for the semiconducting (OFF) state of VO₂ as well as for the metallic state (ON) of VO₂. Subsequently, the near-field ISR was calculated by taking the ratio ($I_{\text{ON}}/I_{\text{OFF}}$) of the intensity enhancement in the ON (metallic VO₂) state of the switch to its OFF (semiconducting VO₂) state, for the different cases discussed in this section.

3.1. Effect of increasing the fractal order

Figure 2 shows the near-field intensity enhancement and the variation of the ISR with wavelength—for the proposed plasmonic fractal nanoantenna based near-field switch—with increasing fractal order. Figure 2(a) shows the near-field intensity enhancement versus wavelength at the center of the nanoantenna for fractal order 0 of the proposed switch. It can be seen that when VO₂ is present in its metallic state, the plasmonic mode is present at a wavelength of ~ 1940 nm. However, when the VO₂ is present in its semiconducting state, the strongest plasmonic mode shifts to higher wavelengths beyond 2500 nm, along with the appearance of additional weak modes at ~ 1720 and ~ 750 nm. Due to these near-field spectral characteristics, there is a creation of a favorable zone for switching around the wavelength of ~ 1250 nm. At this wavelength (marked with a dashed line in figure 2(a)), the switch can be treated as ON when VO₂ is in its metallic state (i.e. VO₂ (M)) as it has a significant intensity enhancement in this wavelength region, and it can be treated as OFF when VO₂ is in its semiconductor state (i.e. VO₂ (S)) as it is in its off-resonance wavelength region. At this wavelength ~ 1250 nm, a maximum ISR of ~ 32 can be obtained with the fractal order zero of the proposed switch. In general, it is expected that the near-field ISR will be highest at the wavelength where the near-field intensity enhancement in the ON state (with VO₂ (M)) is at

its maximum, and that of the OFF state (with VO₂ (S)) is at its minimum.

However, as the fractal order increases, a significant increase in the ISR can be obtained. Figure 2(b) shows that, for VO₂ in its metallic state, the switch with a fractal order 1 displays a higher intensity enhancement, compared to the intensity enhancement obtained with the case with fractal order 0. Moreover, for VO₂ in its semiconducting state, the switch with fractal order 1 displays a lower off-resonant intensity enhancement compared to the one with fractal order 0. At a wavelength of ~ 1250 nm, this simultaneous enhancement of intensity in the 'ON' state (VO₂ (M)) and a reduction of intensity in the 'OFF' state (VO₂ (S)) leads to a three-fold increase in the maximum ISR (resulting in a value of ISR of ~ 90 at 1250 nm) when the fractal order is increased from 0 to 1.

It must be noted from figure 2(b) that the plasmon resonance wavelengths of the intensity enhancement spectra blue-shift with an increase in the fractal order from 0 to 1 for both the VO₂ (M) and VO₂ (S) states of the proposed switch. The blue-shift is expected due to the redistribution of dipoles across the self-similar structure with an increase in the fractal order. The fractalization alters the polarizability as well as the extinction spectra of the nanoantenna. The reason for this blue-shift is also discussed further in supplementary information, note 3. However, the wavelength of the maximum ISR remains the same for both fractal orders 0 and 1. This can be explained by the overlapping E -field enhancement spectra shown in figure 3(a) where it can be seen that the E -field enhancement ($|\mathbf{E}|/|\mathbf{E}_0|$) at ~ 1250 nm is almost the same for both fractal order 0 and 1 for the switch in its metallic state, as the graphs of E -field enhancement versus wavelength cross each other around this point. Moreover, it can be seen from figure 3(b) that for the semiconducting state of the switch, there is only a slight blue-shift in the E -field enhancement spectrum when the fractal order is changed from 0 to 1.

Figure 2(c) shows that as the fractal order is further increased to 2, there is a yet higher intensity enhancement in the 'ON' state of the switch (i.e. when VO₂ is in its metallic state). Moreover, there is a significant reduction of intensity enhancement in the 'OFF' state of the switch (i.e. when VO₂ is in its semiconductor state), leading to an ISR of ~ 900 at a wavelength of ~ 1170 nm which is ~ 30 times higher than the switch of fractal order 0. It must be noted that the wavelength of maximum ISR in this case is blue-shifted to 1170 nm (as compared to 1250 nm in the case of the lower order fractals) due to the blue-shift in the plasmon resonance wavelengths of the intensity enhancement spectra obtained for VO₂ (M) and VO₂ (S) states, with an increase in the fractal order. Further, figure 3(b) shows that as the fractal order increases, the switch in its semiconducting VO₂ state, starts exhibiting a Fano-like feature in the E -field enhancement spectra. This can be particularly noticed for the fractal order of 2. The E -field enhancement versus wavelength graphs for the proposed near-field switch—with the underlying VO₂ in its metallic and semiconductor state—for an extended wavelength range along with the surface charge density distributions at the respective plasmon resonance wavelengths are given in supplementary information, note 4.

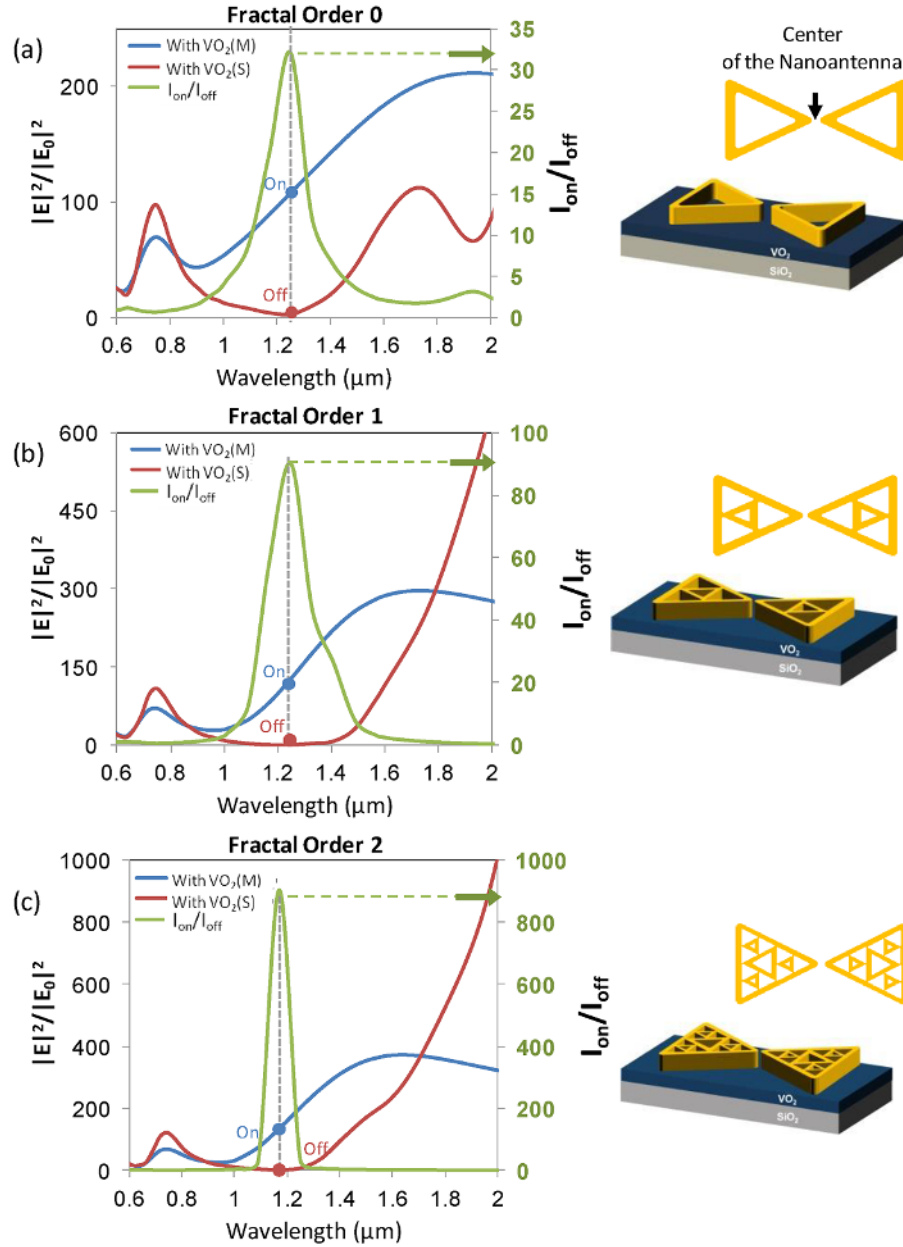


Figure 2. Intensity enhancement ($|E|^2/|E_0|^2$) versus wavelength for the proposed switch with VO₂ in its metallic (M) and semiconductor (S) state for: (a) fractal order 0, (b) fractal order 1, and (c) fractal order 2. The I_{ON}/I_{OFF} ratio is shown on the secondary axis for each case. The ISR, i.e. the I_{ON}/I_{OFF} increases as the fractal order increases. The structural parameters for the near-field switch are taken as length of the nanoantenna arm, $L = 350$ nm; flare angle = 60° ; height, $h = 80$ nm; thickness of the VO₂ layer, $t = 20$ nm; contour thickness, $c = 15$ nm and gap between the triangular antenna segments, $G = 10$ nm.

Figure 4 shows the spatial maps of the E -field enhancement ($|E|/|E_0|$) for the proposed switch for different fractal orders. The maps are shown for the switch—for both the metallic state and the semiconductor state of VO₂—at the wavelengths where maximum ISR is obtained for the respective fractal orders. Figures 4(a)–(c) show that when the switch is in its ON state (i.e. when VO₂ is in its metallic state), the E -field between the two arms of the nanoantenna gets slightly enhanced as the fractal order is increased from 0 to 2 and stays tightly confined at the center. Figures 4(d)–(f) show that, with the switch in its OFF state (i.e. when VO₂ is in its semiconductor state), the

E -field between the two arms of the antenna gets significantly reduced on increasing the fractal order from 0 to 2. This occurs due to the distribution of the EM fields amongst the fractal features. The decrease of the E -field can be seen more clearly in the magnified figures, i.e. in figures 4(g)–(i). Therefore, it can be seen that the near-field switch based on the Sierpiński-fractal contour-bowtie plasmonic nanoantenna on VO₂ exhibits higher values of I_{ON}/I_{OFF} (ISR) for higher fractal orders due to the simultaneous increase of the E -field enhancement in the ON state and the decrease of E -field enhancement in the OFF state as the fractal order is increased.

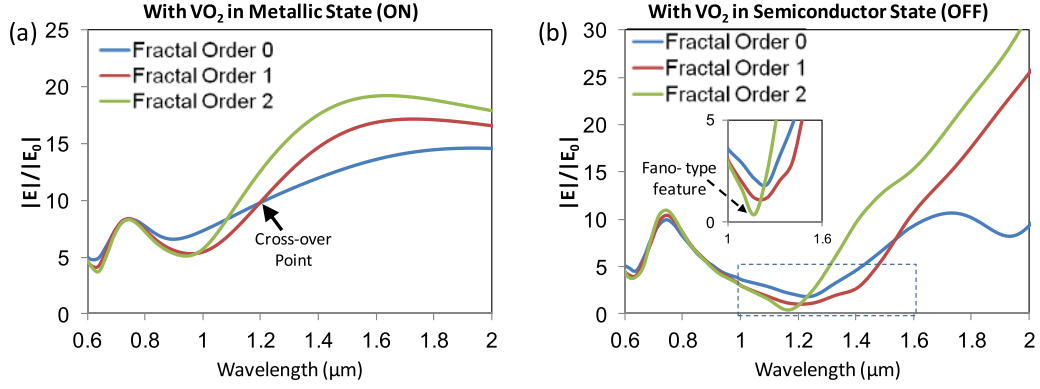


Figure 3. E -field enhancement ($|E|/|E_0|$) versus wavelength graphs for the Sierpiński-fractal contour-bowtie plasmonic nanoantenna on VO_2 for fractal orders 0, 1, and 2 of the fractal nanoantenna with (a) VO_2 in its metallic state and (b) VO_2 in its semiconductor state. The geometrical parameters for the near-field switch are taken as length of the nanoantenna arm, $L = 350$ nm; flare angle $= 60^\circ$; height, $h = 80$ nm; thickness of the VO_2 layer, $t = 20$ nm; contour thickness, $c = 15$ nm and gap between the triangular antenna segments, $G = 10$ nm.

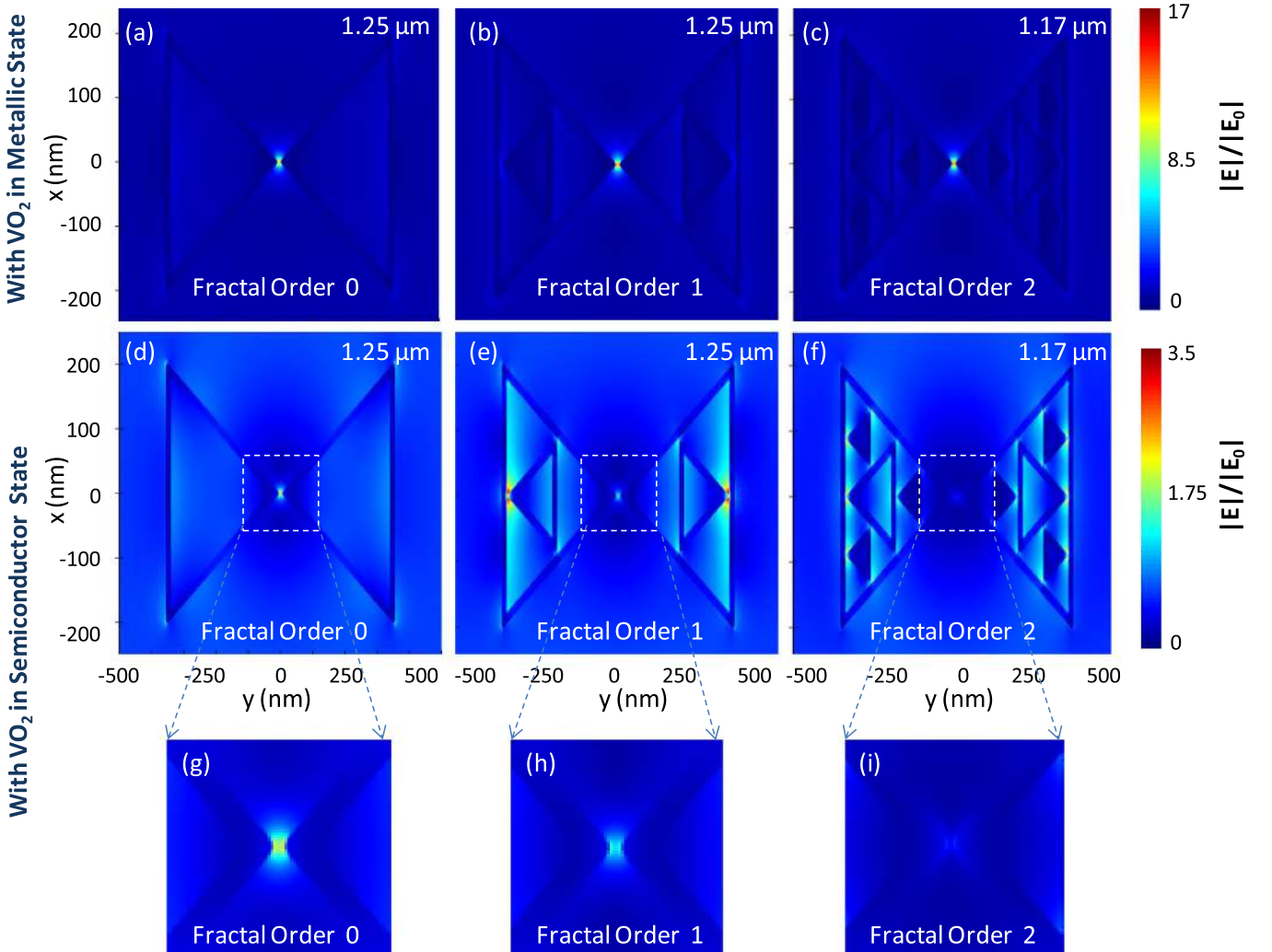


Figure 4. E -field enhancement profiles for the ON (with VO_2 in metallic state) state of the Sierpiński-fractal contour-bowtie plasmonic nanoantenna on VO_2 for (a) fractal order 0 (b) fractal order 1 and (c) fractal order 2 of the fractal nanoantenna. E -field enhancement profiles for the OFF (with VO_2 in semiconductor state) state of the proposed fractal nanoantenna on VO_2 for (d) fractal order 0 (e) fractal order 1 and (f) fractal order 2 of the fractal nanoantenna. (g)–(i) The magnified images for the OFF state are shown for fractal orders 0, 1 and 2 for clarity. The geometrical parameters for the near-field switch are taken as length of the nanoantenna arm, $L = 350$ nm; flare angle $= 60^\circ$; height, $h = 80$ nm; thickness of the VO_2 layer, $t = 20$ nm; contour thickness, $c = 15$ nm and gap between the triangular antenna segments, $G = 10$ nm.

3.2. Effect of the length of the nanoantenna arm (L)

The spectral tunability of the proposed switch was analyzed by carrying out a systematic analysis of the effect of the length of the arm of the nanoantenna (L) on the switching behavior of the switch, i.e. on the maximum ISR, and on the wavelength at which the maximum ISR is obtained. This analysis was also done to optimize the length of the arm of the nanoantenna in order to obtain the maximum ISR. Figure 5 shows the effect of varying the length of the nanoantenna arm (L) from 250 to 375 nm (figure 5(a)) while keeping the flare angle, the contour thickness, the height of the nanoantenna, the thickness of the VO₂ layer, and the gap between the two antenna segments fixed as 60°, 15, 80, 20 and 10 nm, respectively. Figures 5(b) and (c) show the effect of changing the arm length of the nanoantenna on the intensity enhancement spectra for the fractal order 0 when VO₂ is in its metallic and semiconductor states, respectively. It can be seen from figure 5(b) that for the 0th fractal order of the nanoantenna with VO₂ in its metallic state, two plasmonic modes can be observed in the intensity enhancement spectrum—a short wavelength mode (SWM) with lower enhancement and a long wavelength mode (LWM) with higher enhancement. As the length of the nanoantenna arm changes from 250 to 375 nm for the 0th fractal order, a decrease in the value of the maximum intensity enhancement for the LWM can be observed along with a linear red-shift in the position of the resonant wavelength from 1569 nm to a little beyond 2000 nm. This resonance wavelength is expected to red-shift with an increase in the length of the arm of the nanoantenna due to a change in the dipolar polarizability with varying length, and the dependence of the LSP resonance wavelength on the length of the nanoantenna [66]. With VO₂ in its semiconducting state, an analysis of the off-resonance dip is carried out as the switch is expected to be in the OFF, i.e. off-resonance in this state. As the length of the nanoantenna is varied from 250 to 375 nm (figure 5(c)), the off-resonant wavelength varies from 1064 to 1250 nm. For the 1st fractal order with VO₂ in its metallic state, (figure 5(d)), the plasmon resonance wavelength for the LWM changes from 1410 to 1808 nm as the length of the nanoantenna arm increases from 250 to 375 nm. A similar red-shifting is seen for the case when the VO₂ is in its semiconducting state (figure 5(e)). For fractal order 2, the feature size of the fractal structures for ' L ' less than 300 nm becomes too small and cannot be fabricated with the state-of-the-art fabrication facilities. Hence, for fractal order 2, nanoantenna arm lengths less than 300 nm have not been considered. It can be seen from figure 5(f), that for fractal order 2, with VO₂ in its metallic state, the plasmon resonance wavelength for the LWM red shifts from 1516 to 1702 nm, along with a decrease in the maximum intensity enhancement as the antenna arm length is varied from 300 to 375 nm. Further, for fractal order 2, it can be seen from figure 5(g), that as the length of the arm of the nanoantenna increases, there is a red-shift in the wavelength of minimum intensity enhancement for the case when VO₂ is in its semiconducting state.

Figures 6(a)–(c) show the ISR versus wavelength for varying lengths of the nanoantenna arm for the different fractal

orders. As shown in figure 6, the wavelength of maximum switching (i.e. the wavelength at which the ISR is the highest) can be tuned over a wide spectral range by varying the length of the nanoantenna arm. For the fractal order 0, the wavelength of maximum switching can be tuned from 1144 to 1250 nm as the arm length is varied from 250 to 375 nm, as shown in figure 6(a). For fractal order 1, the wavelength of maximum ISR can be tuned from 1064 to 1303 nm as the arm length is varied from 250 to 375 nm, as shown in figure 6(b). For fractal order 2, the wavelength of maximum ISR red shifts from 1091 to 1224 nm on varying the length of the nanoantenna arm from 300 to 375 nm, as shown in figure 6(c). Hence, these nanoantennas can be employed for switching in the desirable wavelength range. It should also be noted that for some lengths of the nanoantenna arm, there are multiple peaks in the ISR ($I_{\text{on}}/I_{\text{off}}$) versus wavelength graph for the fractal orders 0 and 1 as shown in figures 6(a) and (b). These peaks result from the ISR being dependent on the relative rate of increase or decrease of the E -field enhancement with wavelength in the ON (with VO₂ (M)) and OFF (with VO₂ (S)) states of the proposed switch (shown in figures 5(b)–(e)).

Further, it can be clearly seen that for all nanoantenna lengths, the ISR is higher for higher fractal orders. Supplementary information: table 1 tabulates the maximum ISRs and the factors by which the ISR increases with higher fractal orders of the switch compared to the fractal order 0, for varying lengths of the nanoantenna arm. Further, it can be noted that there is an optimal arm length of ~ 325 nm where the highest ISR of ~ 2600 is obtained with fractal order 2. For this length, the maximum ISR increases by ~ 3 times with fractal order 1, and ~ 90 times with fractal order 2 compared to the maximum ISR values achievable without the fractal design (fractal order 0).

3.3. Effect of the thickness of the VO₂ thin film (t)

Figure 7 shows the effect of thickness (t) of the underlying VO₂ layer on the switching characteristics of the switch. For this analysis, the length of the nanoantenna arm, the flare angle, the contour thickness, the height of the nanoantenna, and the gap between the two nanoantenna segments were fixed as 350 nm, 60°, 15, 80 and 10 nm, respectively. It can be seen from figures 7(b)–(d) that as the thickness of VO₂ layer is increased from 10 to 100 nm—for different fractal orders—the magnitude of the ISR, i.e. $I_{\text{ON}}/I_{\text{OFF}}$ reaches a maxima at an optimum thickness of the VO₂ layer. While the optimum value of the thickness of the VO₂ layer was calculated to be 50 nm for fractal order 0 (figure 7(b)) and 80 nm for fractal order 1 (figure 7(c)), it was determined to be 35 nm for fractal order 2 (figure 7(d)). The different values of optimal thicknesses of the VO₂ layer for different fractal orders are a result of the underlying plasmonic modes for the metallic and semiconductor states of VO₂ for these fractal orders. Figures 7(e)–(g) show the maps for the effect of thickness of the VO₂ layer on the ISR and the wavelength of maximum ISR for different fractal orders. It can be seen from these figures that

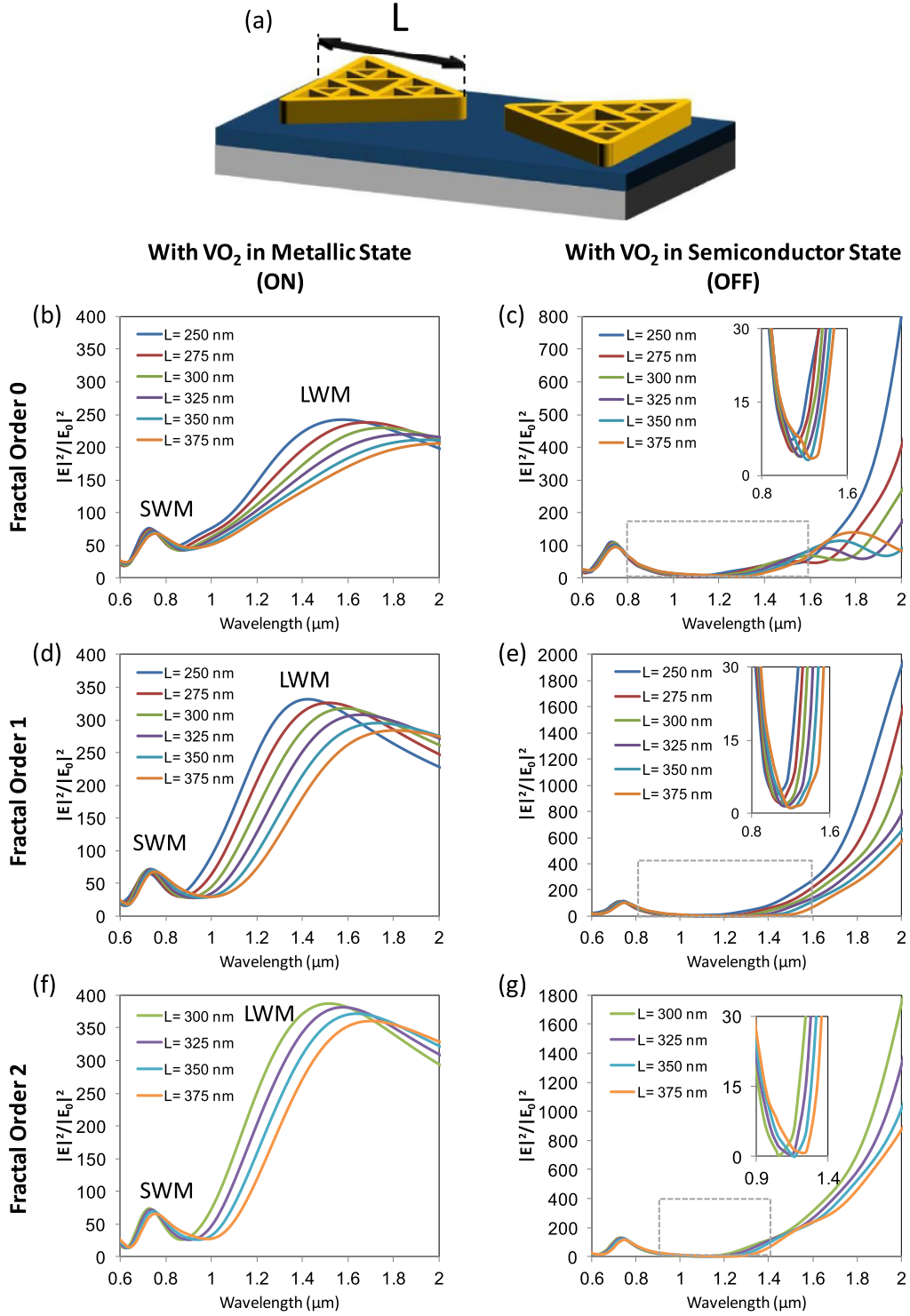


Figure 5. (a) Effect of the length of the nanoantenna arm, ‘L’, of the Sierpiński-fractal contour-bowtie plasmonic nanoantenna on VO₂, on the intensity enhancement ($|E|^2/|E_0|^2$) spectra for fractal order 0 of the fractal nanoantenna when (b) VO₂ is in its metallic state and (c) VO₂ is in its semiconducting state; for fractal order 1 of the fractal nanoantenna when (d) VO₂ is in its metallic state and (e) VO₂ is in its semiconducting state; and for fractal order 2 of the fractal nanoantenna when (f) VO₂ is in its metallic state and (g) VO₂ is in its semiconducting state. The geometrical parameters for the near-field switch are taken as flare angle = 60° height, $h = 80$ nm; thickness of the VO₂ layer, $t = 20$ nm; contour thickness, $c = 15$ nm and gap between the triangular antenna segments, $G = 10$ nm.

the ISR consistently increases as the fractal order is changed from 0 to 2 irrespective of the thickness of the VO₂ layer. This result is in agreement with the fact that higher fractal

orders of the contour-bowtie based nanoantennas give rise to a higher near-field ISR. In addition, it can be observed that for all fractal orders of the proposed switch, there is a red shift

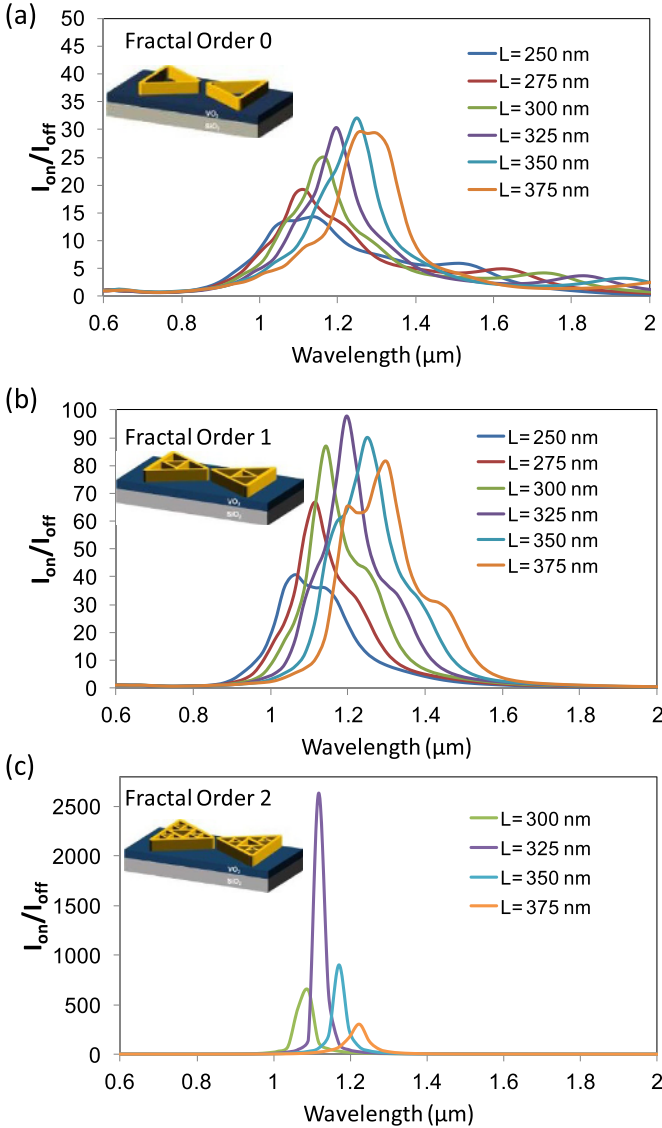


Figure 6. Effect of length ' L ' on the I_{ON}/I_{OFF} ratio (ISR) versus wavelength for the proposed near-field switch for: (a) fractal order 0, (b) fractal order 1, and (c) fractal order 2 of the fractal nanoantenna. The structural parameters for the near-field switch are taken as flare angle = 60° height, $h = 80$ nm; thickness of the VO_2 layer, $t = 20$ nm; contour thickness, $c = 15$ nm and gap between the triangular antenna segments, $G = 10$ nm.

in the wavelength of maximum switching (i.e. the wavelength at which the ISR is the highest) as the thickness of the VO_2 layer is increased. As the thickness of the VO_2 layer is varied from 10 to 100 nm, the wavelength of maximum switching red shifts from 1117 to 1543 nm for fractal order 0, from 1224 to 1596 nm for fractal order 1, and from 1064 to 1543 nm for fractal order 2. The change in magnitude of the ISR and the red-shift in the value of the maximum ISR can be explained by figure 8.

Figures 8(a), (c) and (e) show the effect of the thickness of the VO_2 layer on the E -field enhancement versus wavelength for the fractal orders 0–2, respectively, when VO_2 is in its

metallic state. It can be seen from the figures that the interaction of the contour-bowtie nanoantenna (and its fractal orders) with the underlying VO_2 layer on a SiO_2 substrate, leads to the presence of two plasmonic modes in the E -field enhancement spectra—a LWM (M2) and a SVM (M1). The SVM red-shifts, whereas the LWM blue-shifts as the thickness of the VO_2 (M) layer increases. This behavior can be understood by using an effective medium theory for the VO_2 (M)-on-top-of- SiO_2 substrate (i.e. the combination of the VO_2 film and the SiO_2 substrate) on which the gold nano-antenna is placed. It is well known the permittivity of SiO_2 is positive [67]. However, the permittivity of VO_2 in its metallic state is negative above 1130 nm. Thus, using the effective medium theory, it can be deduced that the permittivity of the effective substrate (VO_2 (M)-on-top-of- SiO_2) will be less than that of SiO_2 after a certain wavelength point. Further, as the thickness of the VO_2 layer is increased, the value of the wavelength above which the permittivity of the effective substrate will be less than that of SiO_2 will get blue-shifted. This will lead to the creation of a transition point at 1130 nm above which the effective permittivity will decrease with an increase in the VO_2 layer thickness, and below which the effective permittivity will increase with an increase in the VO_2 layer thickness. As the SVM occurs below a wavelength of 1130 nm, it displays a red-shift as the value of the effective permittivity of the underlying substrate increases with an increase in the VO_2 layer thickness. On the other hand, the longer wavelength mode that occurs at a wavelength above 1130 nm exhibits a blue-shift as the value of the effective permittivity decreases with an increase in the VO_2 layer thickness. This effect can be seen for all fractal orders. Further it should be noted that as the VO_2 layer thickness increases from 10 to 40 nm, there is a decrease in the E -field enhancement of the long-wavelength plasmonic mode due to an increase in the imaginary part of the permittivity of the effective medium. However, as the thickness is increased beyond 40 nm, the increase in the loss due to the imaginary part of the permittivity is offset by the possible increase in reflectance from the substrate, thus leading to an increase in the E -field enhancement. Moreover, the shorter wavelength mode also displays an increase in the E -field enhancement with an increase in the thickness of the VO_2 layer. Figures 8(b), (d) and (f) show the effect of the thickness of the VO_2 layer on the E -field enhancement versus wavelength for the fractal orders 0–2 respectively, when VO_2 is in its semiconductor state. As the permittivity of VO_2 in its semiconductor state is positive, the off-resonance wavelengths (i.e. the dips in the E -field enhancement spectra) and the on-resonance (plasmonic mode) wavelengths undergo a red-shift due to the increase in the effective permittivity with an increase in the VO_2 layer thickness. It must be noted from figures 8(d) and (f) that for fractal orders 1 and 2, the plasmonic mode occurs at a wavelength beyond $2 \mu\text{m}$, hence, the red-shift can be seen only in the off-resonance wavelength. The effect of the thickness of the VO_2 layer on the ISR versus wavelength curves is further discussed in the supplementary information, note 5 (figure S5), for the various fractal orders of the proposed switch.

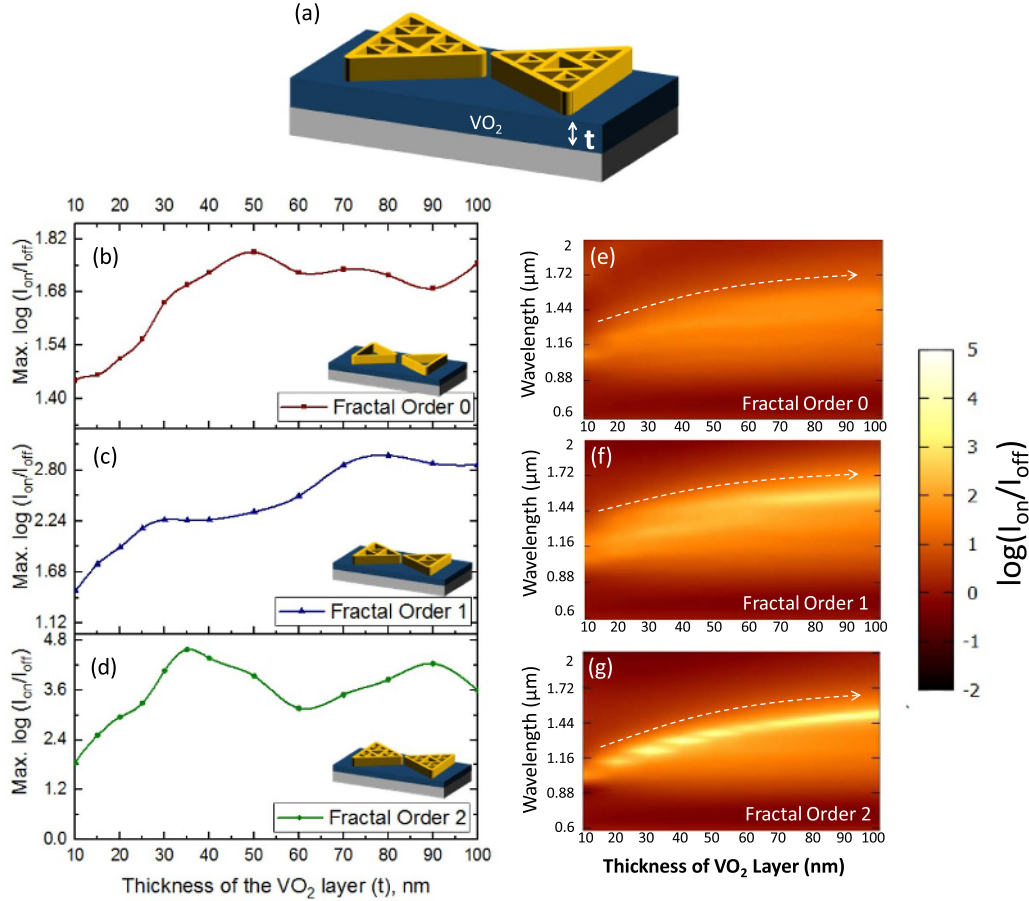


Figure 7. (a) Schematic showing the thickness ‘ t ’ of the VO₂ layer in a near-field plasmonic switch based on a Sierpiński-fractal nanoantenna on a VO₂ film. Effect of the thickness of the VO₂ layer on the maximum I_{on}/I_{off} ratio for (b) fractal order 0 (c) fractal order 1, and (d) fractal order 2 of the fractal structure. I_{on}/I_{off} maps for the near-field switch as a function of thickness of the VO₂ layer and wavelength for: (e) Fractal order 0, (f) fractal order 1, and (g) fractal order 2 of the fractal nanoantenna. The structural parameters for the near-field switch are taken as flare angle = 60° height, $h = 80$ nm; length of the nanoantenna arm, $L = 350$ nm; contour thickness, $c = 15$ nm and gap between the triangular antenna segments, $G = 10$ nm.

3.4. Effect of the contour-thickness (c) of the nanoantenna

Figure 9 shows the effect of the contour thickness, ‘ c ’, of the nanoantenna on the ISR for fractal orders 0–2. The contour thickness of these nanoantennas can be varied to obtain a wide spectral tunability while keeping the length of the nanoantenna arm constant. It can be seen from the inset of figure 9(b), that for the 0th fractal order, the wavelength of maximum ISR blue-shifts from 1410 to 1064 nm as the contour thickness is increased from 10 to 30 nm in steps of 5 nm. The effect of the contour thickness on the plasmonic behavior of the proposed switch can be analyzed by employing the plasmon hybridization model [68, 69]. In a hollow contour bowtie nanoantenna, the induced surface charges of the nanoantenna result from the interaction of the solid and the cavity bowtie antenna plasmons excited by the incident electromagnetic radiation. The strength of interaction between the solid and cavity bowtie antenna plasmons is heavily dependent on the thickness of the metallic contour layer. As the contour thickness is decreased, the interaction between the solid and cavity bowtie plasmons is expected to become stronger, thus leading to the splitting of the plasmon resonance into new modes. The effect of contour

thickness on the E -field enhancement spectra for the different fractal orders of the proposed switch, for both metallic and semiconductor states of underlying VO₂, are shown in figure S6 (see supplementary information, note 6). The reduction of the contour thickness gives rise to multiple weak modes which can be visualized for lower contour thicknesses in figure S6(b) for fractal order 0. As the ISR (I_{on}/I_{off}) is a ratio of the intensity enhancement of the switch with VO₂ in the metallic state to that of the switch with VO₂ in its semiconductor state, the multiple weak modes for lower values of contour thickness show up as multiple peaks in figure 9(b). Additionally, the strength of coupling and the energy between the plasmons on the inner and outer contour structures determine the shift of the hybridization plasmon energy. As the contour thickness is increased, the strength of coupling decreases, thus leading to a blue shift in the plasmon resonance wavelength. It can be seen from figure S6 that the plasmonic mode (on-resonance wavelength) of the VO₂ (M) state and the off-resonance wavelength of the VO₂ (S) state both undergo a blue-shift with an increase in the thickness of the contour. Moreover, it can be seen from figure 9(b) that there is an optimal thickness of 15 nm at which the maximum ISR is obtained. Figure 9(c) shows that for the

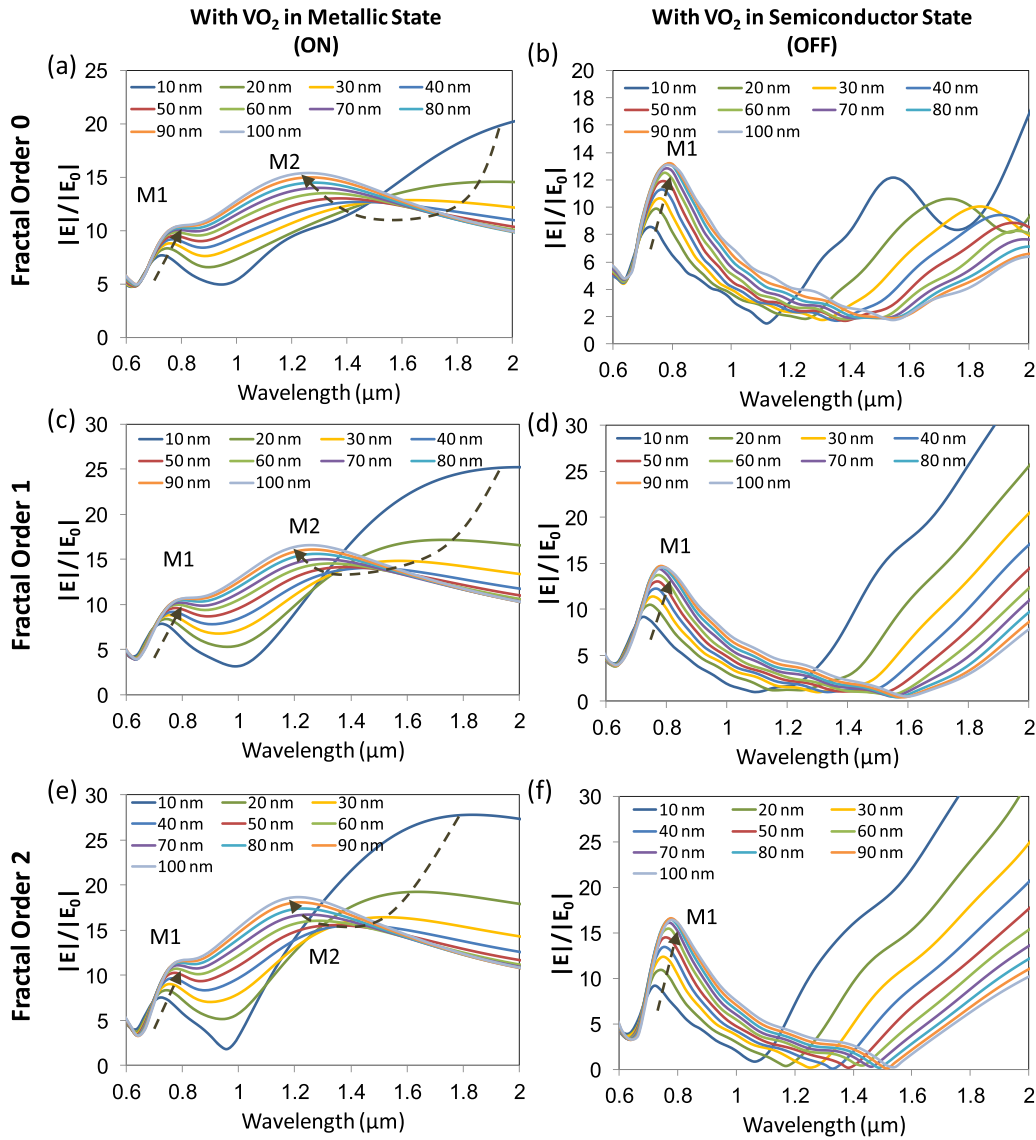


Figure 8. Effect of the thickness of the VO₂ layer on the E -field enhancement ($|E|/|E_0|$) for—fractal order 0 of the fractal structure when (a) VO₂ is in its metallic state and (b) VO₂ is in its semiconducting state; for fractal order 1 of the fractal structure with (c) VO₂ is in its metallic state and (d) VO₂ is in its semiconducting state; and for fractal order 2 when (e) VO₂ is in its metallic state and (f) VO₂ is in its semiconducting state. The geometrical parameters for the near-field switch are taken as flare angle = 60° height, $h = 80$ nm; length of the nanoantenna arm, $L = 350$ nm; contour thickness, $c = 15$ nm and gap between the triangular antenna segments, $G = 10$ nm.

fractal order being 1, the wavelength of maximum ISR blue shifts from 1277 to 1091 nm as the thickness of the contour increases from 10 to 30 nm. In addition, the maximum ISR is obtained for a contour thickness of 30 nm for fractal order 1. For fractal order 2, contour thickness higher than 20 nm has not been considered as it is not possible to fabricate fractal features of order 2 of the proposed switch with thickness of the contour greater than 20 nm. Figure 9(d) shows that for the fractal order 2, the maximum ISR is achieved at a contour thickness of 10 nm for fractal order 2. Further, the wavelength of maximum ISR blue shifts from 1303 to 1117 nm as the thickness of the contour increases from 10 to 20 nm. Thus, it can be concluded that for all fractal orders, a variation in the contour thickness may also be used to obtain tunability of the wavelength of maximum ISR.

These near-field switches based on Sierpiński-fractal contour-bowtie plasmonic nanoantenna on VO₂ could also be employed for the visible range by optimizing the value of geometrical parameters of the plasmonic nanoantenna. For possible operation in the visible spectral regime, the length of the nanoantenna arm can be reduced. In addition, employing a higher value of the contour thickness can also lead to the blue-shifting of the wavelength of maximum ISR to the visible region of the spectrum. Moreover, modified Sierpiński-fractal nanoantennas can be explored for operation of the near-field switches in the visible spectral regime. Further, designs of nanoantenna based on fractals other than the Sierpiński-fractal such as the Koch fractal nanoantenna or the Cayley fractal nanoantenna on VO₂-coated substrates could be explored for near-field switching in the visible or the near-IR range.

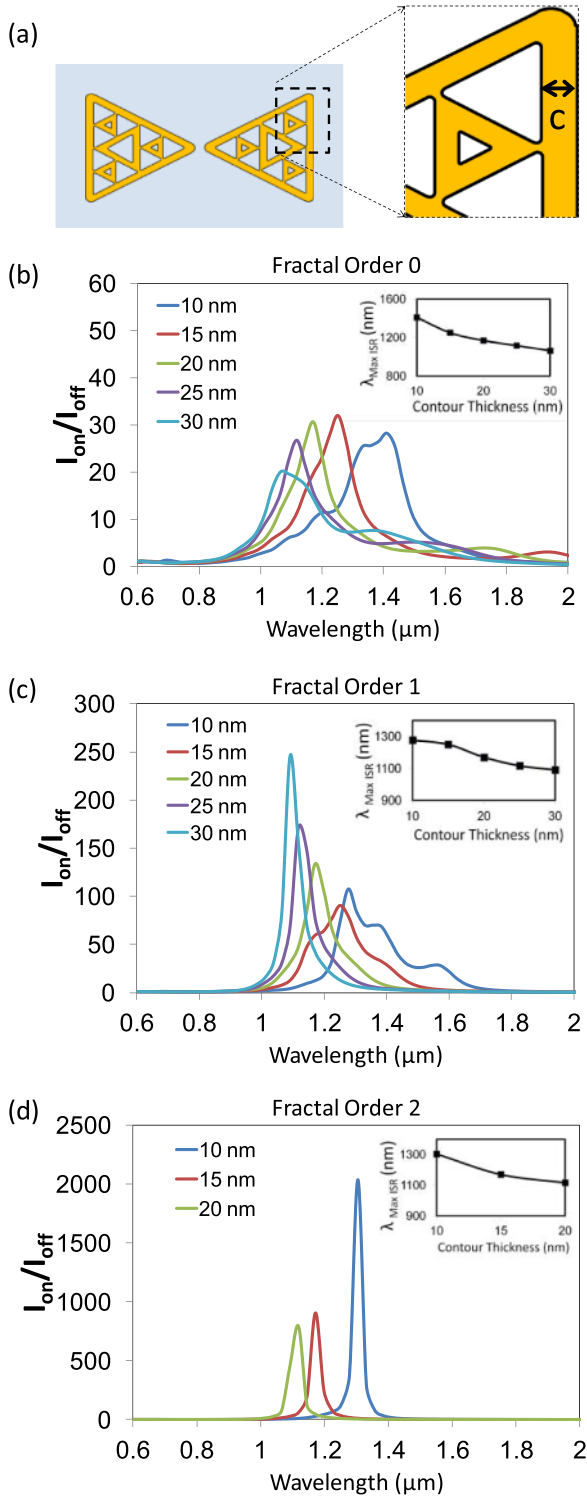


Figure 9. (a) Schematic showing the contour thickness, c , of the proposed plasmonic nanoantenna. Effect of contour thickness of the proposed nanoantenna on the I_{on}/I_{off} ratio (ISR) for (b) fractal order 0, (c) fractal order 1 and (d) fractal order 2 of the fractal structure. The insets show the variation of the wavelength of maximum ISR (I_{on}/I_{off}) with contour thickness. The structural parameters for the near-field switch are taken as flare angle = 60° height, $h = 80$ nm; thickness of the VO_2 layer, $t = 20$ nm, length of the nanoantenna arm, $L = 350$ nm; and gap between the triangular antenna segments, $G = 10$ nm.

4. Conclusion

In this paper, Sierpiński-fractal contour-bowtie plasmonic nanoantennas on top of a VO_2 (vanadium-dioxide) thin film have been proposed for active near-field plasmonic switching. We employed FDTD simulations to determine that higher fractal orders of the proposed plasmonic fractal nanoantennas lead to a significant increase in the near-field ISR that can be achieved by employing these nanoantennas. We report a near-field ISR of ~ 900 by employing a fractal order 2 of the proposed nanoantenna on a VO_2 thin film, which is the highest value of ISR reported thus far for a near-field plasmonic switch. Moreover, it was found that a yet higher value of ISR of ~ 2600 can be obtained for an optimal length of the nanoantenna arm (L), i.e. 325 nm. Further, as the length of the nanoantenna arm is varied from 250 to 375 nm, the wavelength of maximum switching (i.e. the wavelength at which the ISR is the highest) can be tuned from 1144 to 1250 nm and from 1064 to 1303 nm for fractal order 0 and fractal order 1, respectively. For fractal order 2, the wavelength of maximum switching can be tuned from 1091 to 1224 nm on varying the length of the nanoantenna arm from 300 to 375 nm. Further, it was observed that the wavelength of maximum ISR can be red shifted by over 350 nm with an increase in the thickness of the VO_2 layer from 10 to 100 nm, for all fractal orders. In addition, an optimal value of the VO_2 thickness for maximum ISR was calculated for fractal orders 0, 1, and 2. We also observed that the contour thickness of these nanoantennas can also be varied to obtain a wide spectral tunability while keeping the length of the nanoantenna arm constant.

Data availability statement

The data that support the findings of this study are available upon reasonable request from the authors.

Acknowledgments

Above all, A D and Y S would like to thank Lord Jesus for blessing this work. This research was supported in part by the Visvesvaraya PhD Scheme of Ministry of Electronics and Information Technology, Government of India, being implemented by Digital India Corporation (formerly Media Lab Asia). It was also supported by the Ministry of Human Resource Development (MHRD) (RP03417G: IMPRINT Program), the Science and Engineering Research Board (SERB) (RP03932G), and the Defense Research and Development Organization (DRDO) (RP03356G, RP03436G, and RP03437G).

ORCID iDs

Yashna Sharma <https://orcid.org/0000-0002-3405-7895>

Anuj Dhawan <https://orcid.org/0000-0001-5245-7713>

References

- [1] Maier S A 2007 *Plasmonics: Fundamentals and Applications* (Boston, MA: Springer)
- [2] Novotny L and Hecht B 2006 *Principles of Nano-Optics* (New York: Cambridge University Press)
- [3] Greybush N J, Pacheco-Peña V, Engheta N, Murray C B and Kagan C R 2019 Plasmonic optical and chiroptical response of self-assembled Au nanorod equilateral trimers *ACS Nano* **13** 1617–24
- [4] Mohammadi Estakhri N, Edwards B and Engheta N 2019 Inverse-designed metastructures that solve equations *Science* **363** 1333–8
- [5] La Spada L, Spooner C, Haq S and Hao Y 2019 Curvilinear metasurfaces for surface wave manipulation *Sci. Rep.* **9** 1–10
- [6] Lalegani Z, Ebrahimi S S, Hamawandi B, La Spada L and Toprak M S 2020 Modeling, design, and synthesis of gram-scale monodispersed silver nanoparticles using microwave-assisted polyol process for metamaterial applications *Opt. Mater.* **108** 110381
- [7] Akbari M, Shahbazzadeh M J, La Spada L and Khajehzadeh A 2021 The graphene field effect transistor modeling based on an optimized ambipolar virtual source model for DNA detection *Appl. Sci.* **11** 8114
- [8] Sharma Y, Tiruveedhula V A, Muth J F and Dhawan A 2015 VO₂ based waveguide-mode plasmonic nano-gratings for optical switching *Opt. Express* **23** 5822–49
- [9] La Spada L and Vegni L 2017 Near-zero-index wires *Opt. Express* **25** 23699–708
- [10] Mario A and Alù A 2012 *Optical Antennas* (Cambridge: Cambridge University Press)
- [11] Giannini V, Fernández-Domínguez A I, Heck S C and Maier S A 2011 Plasmonic nanoantennas: fundamentals and their use in controlling the radiative properties of nanoemitters *Chem. Rev.* **111** 3888–912
- [12] Habib A, Zhu X, Fong S and Yanik A A 2020 *Active plasmonic nanoantenna: an emerging toolbox from photonics to neuroscience* *Nanophotonics* **9** 3805–29
- [13] Kühler P, Roller E M, Schreiber R, Liedl T, Lohmüller T and Feldmann J 2014 Plasmonic DNA-origami nanoantennas for surface-enhanced Raman spectroscopy *Nano Lett.* **14** 2914–9
- [14] Kinkhabwala A, Yu Z, Fan S, Avlasevich Y, Müllen K and Moerner W E 2009 Large single-molecule fluorescence enhancements produced by a bowtie nanoantenna *Nat. Photon.* **3** 654–7
- [15] Roxworthy B J, Ko K D, Kumar A, Fung K H, Chow E K, Liu G L, Fang N X and Toussaint J K C 2012 Application of plasmonic bowtie nanoantenna arrays for optical trapping, stacking, and sorting *Nano Lett.* **12** 796–801
- [16] Pfullmann N *et al* 2013 Bow-tie nano-antenna assisted generation of extreme ultraviolet radiation *New J. Phys.* **15** 093027
- [17] Bicket I C, Bellido E P, McRae D M, Lagugne-Labarthe F and Botton G A 2020 Hierarchical plasmon resonances in fractal structures *ACS Photonics* **7** 1246–54
- [18] Bicket I C, Bellido E P, McRae D M, Lagugne-Labarthe F and Botton G A 2019 Carving plasmon modes in silver Sierpiński fractals *ACS Photonics* **6** 2974–84
- [19] de Nicola F, Puthiya Purayil N S, Spirito D, Miscuglio M, Tantussi F, Tomadin A, de Angelis F, Polini M, Krahne R and Pellegrini V 2018 Multiband plasmonic Sierpiński carpet fractal antennas *ACS Photonics* **5** 2418–25
- [20] Sederberg S and Elezzabi A Y 2011 Sierpiński fractal plasmonic antenna: a fractal abstraction of the plasmonic bowtie antenna *Opt. Express* **19** 10456–61
- [21] Gottheim S, Zhang H, Govorov A O and Halas N J 2015 Fractal nanoparticle plasmonics: the Cayley tree *ACS Nano* **9** 3284–92
- [22] Hegde R S and Khoo E H 2016 Broadband optical response in ternary tree fractal plasmonic nanoantenna *Plasmonics* **11** 465–73
- [23] Bellido E P, Bernasconi G D, Rossouw D, Butet J, Martin O J and Botton G A 2017 Self-similarity of plasmon edge modes on Koch fractal antennas *ACS Nano* **11** 11240–9
- [24] Cakmakyan S, Cinel N A, Cakmak A O and Ozbay E 2014 Validation of electromagnetic field enhancement in near-infrared through Sierpiński fractal nanoantennas *Opt. Express* **22** 19504–12
- [25] Aslan E, Aslan E, Wang R, Hong M K, Erramilli S, Turkmen M, Saracoglu O G and Dal Negro L 2016 Multispectral Cesaro-type fractal plasmonic nanoantennas *ACS Photonics* **3** 2102–11
- [26] Zhu L H, Shao M R, Peng R W, Fan R H, Huang X R and Wang M 2013 Broadband absorption and efficiency enhancement of an ultra-thin silicon solar cell with a plasmonic fractal *Opt. Express* **21** 313–23
- [27] Kazerooni H and Khavasi A 2014 Plasmonic fractals: ultrabroadband light trapping in thin film solar cells by a Sierpiński nanocarpenter *Opt. Quantum Electron.* **46** 751–7
- [28] Volpe G, Volpe G and Quidant R 2011 Fractal plasmonics: subdiffraction focusing and broadband spectral response by a Sierpiński nanocarpenter *Opt. Express* **19** 3612–8
- [29] Chen J, Li Z, Zhang X, Xiao J and Gong Q 2013 Submicron bidirectional all-optical plasmonic switches *Sci. Rep.* **3** 1–6
- [30] Sorger V J, Oulton R F, Ma R M and Zhang X 2012 Toward integrated plasmonic circuits *MRS Bull.* **37** 728–38
- [31] Alaei R, Albooyeh M, Tretyakov S and Rockstuhl C 2016 Phase-change material-based nanoantennas with tunable radiation patterns *Opt. Lett.* **41** 4099–102
- [32] Michel A K U, Zalden P, Chigrin D N, Wuttig M, Lindenberg A M and Taubner T 2014 Reversible optical switching of infrared antenna resonances with ultrathin phase-change layers using femtosecond laser pulses *ACS Photonics* **1** 833–9
- [33] Gupta N, Savaliya P B and Dhawan A 2020 Plasmonic nanoantennas on VO₂ films for active switching of near-field intensity and radiation from nanoemitters *Opt. Express* **28** 27476–94
- [34] Kim S J *et al* 2017 Active directional switching of surface plasmon polaritons using a phase transition material *Sci. Rep.* **7** 1–8
- [35] Erickson D, Serey X, Chen Y F and Mandal S 2011 Nanomanipulation using near field photonics *Lab Chip* **11** 995–1009
- [36] Zhang Y, Liu W, Gao J and Yang X 2018 Generating focused 3D perfect vortex beams by plasmonic metasurfaces *Adv. Opt. Mater.* **6** 1701228
- [37] Metzger B, Hentschel M and Giessen H 2017 Probing the near-field of second-harmonic light around plasmonic nanoantennas *Nano Lett.* **17** 1931–7
- [38] Kohoutek J, Bonakdar A, Gelfand R, Dey D, Hassani Nia I, Fathipour V, Memis O G and Mohseni H 2012 Integrated all-optical infrared switchable plasmonic quantum cascade laser *Nano Lett.* **12** 2537–41
- [39] Matz R, Bauer J G, Clemens P, Heise G, Mahlein H F, Metzger W, Michel H and Schulte-Roth G 1994 Development of a photonic integrated transceiver chip for WDM transmission *IEEE Photonics Technol. Lett.* **6** 1327–9
- [40] Yoo S J B 2008 Photonic integrated circuits for communications, signal processing, and computing applications *Integrated Photonics and Nanophotonics Research and Applications* (Optical Society of America)

- [41] Ghosh R R and Dhawan A 2021 Integrated non-volatile plasmonic switches based on phase-change-materials and their application to plasmonic logic circuits *Sci. Rep.* **11** 1–13
- [42] Passian A and Imam N 2019 Nanosystems, edge computing, and the next generation computing systems *Sensors* **20** 4048
- [43] Brixner T, García de Abajo F J, Schneider J, Spindler C and Pfeiffer W 2006 Ultrafast adaptive optical near-field control *Phys. Rev. B* **73** 125437
- [44] Aeschlimann M *et al* 2012 Optimal open-loop near-field control of plasmonic nanostructures *New J. Phys.* **14** 033030
- [45] Stefanovich G, Pergament A and Stefanovich D 2000 Electrical switching and Mott transition in VO₂ *J. Phys.: Condens. Matter* **12** 8837–45
- [46] Suh J Y, Lopez R, Feldman L C and Haglund J R F 2004 Semiconductor to metal phase transition in the nucleation and growth of VO₂ nanoparticles and thin films *J. Appl. Phys.* **96** 1209–13
- [47] Leroux C, Nihoul G and van Tendeloo G 1998 From VO₂ (B) to VO₂ (R): theoretical structures of VO₂ polymorphs and *in situ* electron microscopy *Phys. Rev. B* **57** 5111
- [48] Beck M, Hofstetter D, Aellen T, Faist J, Oesterle U, Ilegems M and Melchior H 2002 Continuous wave operation of a mid-infrared semiconductor laser at room temperature *Science* **295** 301–5
- [49] Becker M F, Buckman A B, Walser R M, Lépine T, Georges P and Brun A 1994 Femtosecond laser excitation of the semiconductor-metal phase transition in VO₂ *Appl. Phys. Lett.* **65** 1507–9
- [50] Markov P, Marvel R E, Conley H J, Miller K J, Haglund J R F and Weiss S M 2015 Optically monitored electrical switching in VO₂ *ACS Photonics* **2** 1175–82
- [51] Mulchandani K, Soni A, Pathy K and Mavani K R 2021 Structural transformation and tuning of electronic transitions by W-doping in VO₂ thin films *Superlattices Microstruct.* **154** 106883
- [52] Jepsen P U, Fischer B M, Thoman A, Helm H, Suh J Y, Lopez R, Feldman L C and Haglund R F 2006 Metal-insulator phase transition in a VO₂ thin film observed with terahertz spectroscopy *Phys. Rev. B* **74** 205103
- [53] Cavalleri A, Tóth C, Siders C W, Squier J A, Ráksi F, Forget P and Kieffer J C 2001 Femtosecond structural dynamics in VO₂ during an ultrafast solid-solid phase transition *Phys. Rev. Lett.* **87** 237401
- [54] Park J B, Lee I M, Lee S Y, Kim K, Choi D, Song E Y and Lee B 2013 Tunable subwavelength hot spot of dipole nanostructure based on VO₂ phase transition *Opt. Express* **21** 15205–12
- [55] Large N, Abb M, Aizpurua J and Muskens O L 2010 Photoconductively loaded plasmonic nanoantenna as building block for ultracompact optical switches *Nano Lett.* **10** 1741–6
- [56] Savaliya P B, Thomas A, Dua R and Dhawan A 2017 Tunable optical switching in the near-infrared spectral regime by employing plasmonic nanoantennas containing phase change materials *Opt. Express* **25** 23755–72
- [57] Ding W, Bachelot R, Kostcheev S, Royer P and Espiau de Lamaestre R 2010 Surface plasmon resonances in silver Bowtie nanoantennas with varied bow angles *J. Appl. Phys.* **108** 124314
- [58] Hasan D, Ho C P and Lee C 2016 Realization of fractal-inspired thermoresponsive quasi-3D plasmonic metasurfaces with EOT-like transmission for volumetric and multispectral detection in the mid-IR region *ACS Omega* **1** 818–31
- [59] Taflov A and Hagness S C 2000 *Computational Electrodynamics: The Finite-Difference Time-Domain Method* (Boston, MA: Artech House)
- [60] Soltani M, Chaker M, Haddad E, Krizelecky R V and Nikanpour D 2004 Optical switching of vanadium dioxide thin films deposited by reactive pulsed laser deposition *J. Vac. Sci. Technol.* **22** 859–64
- [61] Wang X, Xu J, Fei Y, Li D, Li T, Nie Y, Feng K and Wu N 2002 Preparation of thermochromic VO₂ thin films on fused silica and soda-lime glass by RF magnetron sputtering *Jpn. J. Appl. Phys.* **41** 312
- [62] Sidorkin V, van Veldhoven E, van der Drift E, Alkemade P, Salemink H and Maas D 2009 Sub-10-nm nanolithography with a scanning helium beam *J. Vac. Sci. Technol. B* **27** L18–20
- [63] Fischbein M D and Drndić M 2007 Sub-10 nm device fabrication in a transmission electron microscope *Nano Lett.* **7** 1329–37
- [64] Yeşilyurt A T M and Huang J S 2021 Emission manipulation by DNA origami-assisted plasmonic nanoantennas *Adv. Opt. Mater.* **9** 2100848
- [65] Kim J S and Ahn J 2018 Mask materials and designs for extreme ultra violet lithography *Electron. Mater. Lett.* **14** 533–47
- [66] Khoshdel V and Shokooh-Saremi M 2019 Plasmonic nano bow-tie arrays with enhanced LSPR refractive index sensing *Micro Nano Lett.* **14** 566–71
- [67] Palik E D 1998 *Handbook of Optical Constants of Solids* (New York: Academic)
- [68] Prodan E, Radloff C, Halas N J and Nordlander P 2003 A hybridization model for the plasmon response of complex nanostructures *Science* **302** 419–22
- [69] Nien L W, Lin S C, Chao B K, Chen M J, Li J H and Hsueh C H 2013 Giant electric field enhancement and localized surface plasmon resonance by optimizing contour bowtie nanoantennas *J. Phys. Chem. C* **117** 25004–11